# Ultrafast optomechanical strain in layered GeS

Duan Luo<sup>1,2,3,4</sup>, Baiyu Zhang<sup>5</sup>, Edbert J. Sie<sup>4,6</sup>, Clara M. Nyby<sup>7</sup>, Qingyuan Fan<sup>1,4</sup>, Xiaozhe Shen<sup>2</sup>, Alexander H. Reid<sup>2</sup>, Matthias C. Hoffmann<sup>2</sup>, Stephen Weathersby<sup>2</sup>, Jianguo Wen<sup>8</sup>, Xiaofeng Qian<sup>5</sup>, Xijie Wang<sup>2</sup>, Aaron M. Lindenberg<sup>1,4,9\*</sup>

<sup>1</sup>Department of Materials Science and Engineering, Stanford University, Stanford, CA 94305, USA.

<sup>2</sup>SLAC National Accelerator Laboratory, Menlo Park, CA 94025, USA.

<sup>3</sup>Key Laboratory of Ultra-fast Photoelectric Diagnostics Technology, Xi'an Institute of Optics and Precision Mechanics, Chinese Academy of Sciences, Xi'an 710119, China.

<sup>4</sup>Stanford Institute for Materials and Energy Sciences, SLAC National Accelerator Laboratory, Menlo Park, CA 94025, USA.

<sup>5</sup>Department of Materials Science and Engineering, Texas A&M University, College Station, TX 77843, USA.

<sup>6</sup>Geballe Laboratory for Advanced Materials, Stanford University, Stanford, CA 94305, USA.

<sup>7</sup>Department of Chemistry, Stanford University, Stanford, CA 94305, USA.

<sup>8</sup>Center for Nanoscale Materials, Argonne National Laboratory, Lemont, IL 60439, USA.

<sup>9</sup>Stanford PULSE Institute, SLAC National Accelerator Laboratory, Menlo Park, CA 94025, USA

\*Correspondence to: Aaron M. Lindenberg, aaronl@stanford.edu

KEYWORDS: Optomechanical coupling, 2D materials, strain engineering, photostrictive effect, ultrafast electron diffraction

## ABSTRACT:

Strong coupling between light and mechanical strain forms the foundation for next-generation optical micro- and nano-electromechanical systems. Such optomechanical responses in two-dimensional materials present novel types of functionalities arising from the weak van der Waals bond between atomic layers. Here, by using structure-sensitive mega-electron-volt ultrafast electron diffraction, we report the experimental observation of optically driven ultrafast in-plane strain in the layered group-IV monochalcogenide germanium sulfide (GeS). Surprisingly, the photo-induced structural deformation exhibits strain amplitudes of order 0.1% with ten picosecond fast response time and a significant in-plane anisotropy between zigzag and armchair crystallographic directions. Rather than arising due to heating, experimental and theoretical investigations suggest deformation potentials caused by electronic density redistribution and converse piezoelectric effects generated by photoinduced electric fields are the dominant contributors to the observed dynamic anisotropic strains. Our observations define new avenues for ultrafast optomechanical control and strain engineering within functional devices.

## TEXT:

Optomechanical coupling has recently attracted increasing interest, enabling all-optical direct light-to-mechanical strain conversion<sup>1-7</sup>. Photoinduced nonthermal mechanical deformation of materials shows great promise for wireless and remote optomechanical applications<sup>7, 8</sup> such as photostrictive microactuators<sup>9</sup> and energy harvesting<sup>10-12</sup>. Since its initial discovery in the early 1960s, photostrictive behavior has been widely observed in numerous materials, including ferroelectrics<sup>13-18</sup>, polar<sup>19</sup>/non-polar<sup>20, 21</sup> semiconductors, organic polymers<sup>22, 23</sup>, perovskites<sup>11, 12, 24-26</sup>, transition metal oxides<sup>27</sup>, and ferrites<sup>28</sup>. However, until now, evidence of photostrictive behavior in two-dimensional (2D) materials is scarce, despite their potential for nanoscale and flexible optomechanical applications.

Very recently, a strong in-plane photostrictive effect giving rise to strains on the order of  $10^{-3}$  at excited carrier densities of  $\sim 10^{19}$ /cm<sup>3</sup> has been predicted in a new type of 2D ferroelectric, the monolayer group-IV monochalcogenides<sup>29, 30</sup> (denoted by MX where M=Sn, Ge and X=S, Se, i.e. GeS, SnS, and SnSe), estimated to be an order of magnitude larger than the anomalous responses observed in bulk BiFeO<sub>3</sub> under similar excitation conditions<sup>14, 29, 31</sup>. Layered MX crystals possess a puckered orthorhombic structure with two nonequivalent in-plane orientations: armchair (AC) and zigzag (ZZ) directions (Fig. 1a). For each monolayer, inversion symmetry is broken by a spontaneous lattice strain and puckering,-resulting in a strong in-plane spontaneous polarization along the AC direction (Fig. 1a), alternating layer to layer to form an antiferroelectric structure<sup>32</sup>. Upon photoexcitation, generated free carriers are predicted to couple with the polar lattice to screen the polarization resulting in a reduction of the in-plane dipole moment and compression of the corresponding lattice constant (i.e. a converse piezoelectric effect, CPE)<sup>29</sup>. Thus, as shown in Fig. 1b, the larger lattice vector **b** (AC) of MX exhibits a contraction while the smaller one **a** (ZZ)

expands. Since no experimental studies of photostrictive effects in MX materials have been reported to date, verification of the predicted anisotropic change of lattice parameters and its magnitude and response time is critical for both fundamental and technological reasons. In this work, we use mega-electron-volt ultrafast electron diffraction (MeV-UED) to investigate dynamic light-induced structural changes in a prototypical MX – GeS, exhibiting the largest equilibrium anisotropy ratio of in-plane lattice constants among MXs.

2D layered GeS samples were prepared by mechanically exfoliating a high-quality bulk crystal and subsequently transferred onto standard silicon nitride (SiN) membranes. The sample was excited by a 400 nm fs laser with photon energy above the bandgap and probed by ~100 fs ultrashort electron pulses at normal incidence (Fig. 1c). This configuration provides a direct structural probe of in-plane lattice dynamics following photoexcitation. Fig. 1d shows a typical UED diffraction pattern along the [001] zone axis and reflects the anisotropic orthorhombic crystal structure characteristics of GeS (Top view in Fig. 1b). Bragg reflections originating from the ZZ and AC lattice planes, (h00) and (0k0), are marked with yellow and dark red circles, respectively (Fig. 1d). The reversible photoinduced mechanical deformation of a lattice can be directly obtained from the shift of Bragg peak center positions in reciprocal space, as the change in scattering vector Q ( $Q_{hkl} = \frac{2\pi}{d_{hkl}}$ , where  $d_{hkl}$  is the lattice spacing indexed by Miller indices (hkl)) (Fig. 1e). In addition, this deformation-induced in-plane strain is also reflected in the peak width when an inhomogeneous spatial variation of strain or out-of-plane rippling response<sup>33</sup> is involved.

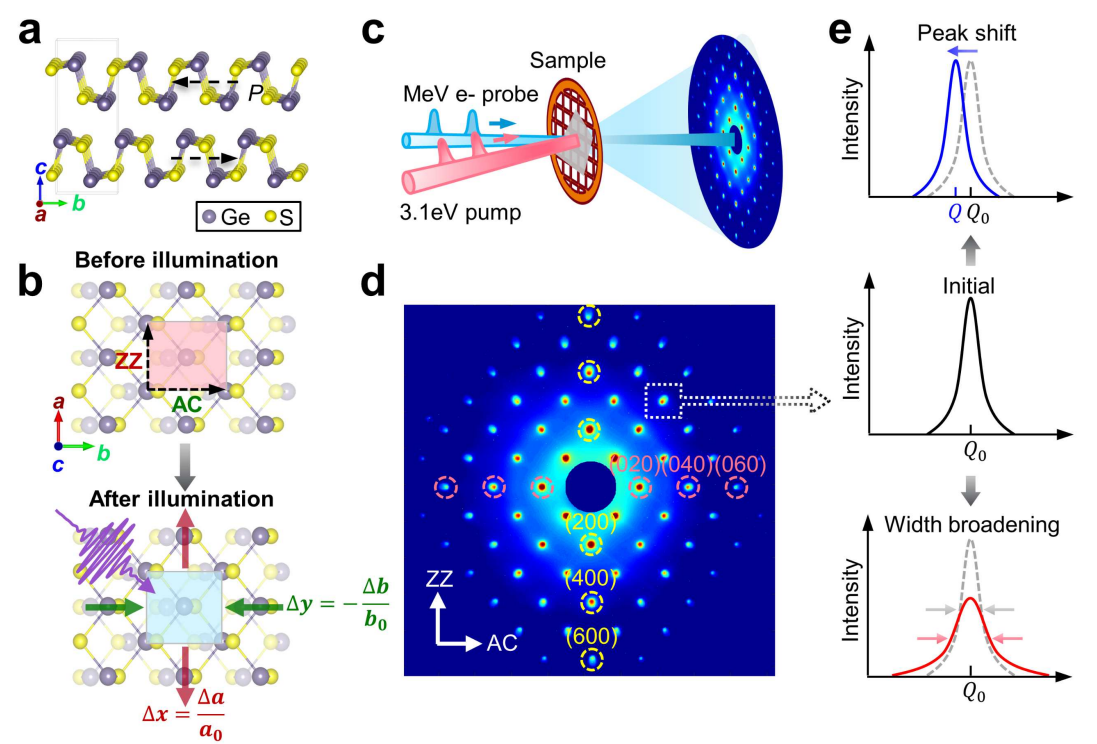


Fig. 1 Anisotropic structure of GeS and schematic illustration of photostriction and UED setup. (a) Side view of the anisotropic crystal structure of GeS. (b) Schematic of photostriction in GeS. Top view of lattice changes before and after illumination. (c) Schematic illustration of

ultrafast electron diffraction. (d) In-plane diffraction pattern of GeS in equilibrium. (e) Schematic 1D profile of diffraction spots shown in (d), illustrating Bragg peak center position and width changes due to lattice deformation after photoexcitation.

To obtain direct information on the mechanical deformation after photoexcitation, we first looked at the 2D differential diffraction pattern by subtracting the UED pattern taken after photoexcitation (t $\approx$ 30 ps) from the pattern before photoexcitation. Surprisingly, clear shifts of the Bragg peaks along the ZZ direction to lower Q (thus ZZ expands) can be observed in the 2D difference map (Fig. 2a and Fig. 2b), while no such obvious shifts were observable in the AC direction. This anisotropy indicates a larger lattice change along the ZZ direction following excitation.

To gain further insight into the evolution of this dynamic process, in particular its magnitude and time scales, we measured time-dependent Q shifts  $(\frac{\Delta Q}{Q_0})$  along the AC and ZZ directions at specific times after the photoexcitation. As shown in Fig. 2d, a significant anisotropy in photo-induced lattice change occurring on different time scales was observed. For ZZ direction, the lattice starts contracting within the first 1.5 ps after light illumination and reaches a maximum contraction of  $\sim 0.4 \times 10^{-3}$  at t $\sim 1.5$  ps. Then, a two-step continuous expansion emerges with a fast expansion on a timescale of  $\sim$ 7 ps and magnitude of 1.1  $\times$  10<sup>-3</sup> followed by a slow expansion rate on a timescale of  $\sim 16$  ps and magnitude of  $0.2 \times 10^{-3}$ . Subsequently, it relaxes to the equilibrium state on a much longer timescale not probed here. In contrast, for the AC direction, the lattice is negligibly changed during the first 7 ps ( $< 10^{-4}$  level), then reaches a maximum lattice compression of  $\sim 0.4 \times 10^{-3}$  at t $\sim 16$  ps, and finally relaxes to its initial state on a longer timescale. Overall, the photostriction-like larger lattice vector (AC) contraction and smaller lattice vector (ZZ) expansion on a 10 ps time scale was observed with a maximum lattice change of  $1.3 \times 10^{-3}$ . Such unusual trends qualitatively align with prior theoretical predictions on monolayer ferroelectric MX<sup>29</sup>, although we investigated multilayer GeS. The 10 ps time scale is among the fastest photostrictive response<sup>15-17</sup> recorded, in particular for in-plane strain.

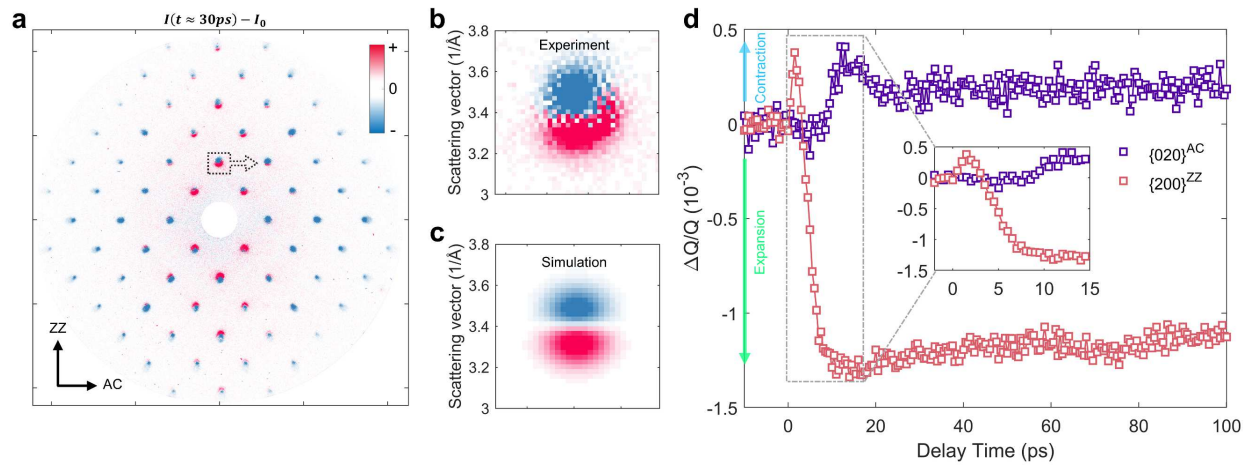


Fig. 2 Ultrafast photo-induced anisotropic strain in GeS. (a) Differential diffraction pattern recorded between before and after (at  $\sim 30$  ps delay time) photoexcitation showing significant Q shifts along the zigzag direction. (b) and (c) Experimental and simulated differential patterns at (200) peak. (d) Measured anisotropic in-plane lattice change with zigzag expansion and armchair contraction occurring on a 10 ps time scale.

To better understand the microscopic mechanism responsible for the anisotropic photostriction behavior, we examine the temporal evolution of the Bragg diffraction intensity by probing reflections (h00), (0k0), and (hk0). For each averaged Friedel pair, a significant anisotropy in the time-dependent diffracted intensity changes for AC and ZZ Bragg reflections is observed (Fig. 3a and Fig. S1). Specifically, these changes can be divided into three major processes – first fast process (t <  $\sim$ 1.5 ps), second slow process (1.5 ps < t <  $\sim$ 20 ps), and third recovery process (t > ~20 ps), which are distinguished by color in light red, light blue, and light grey (Fig. 3a). For AC reflections  $\{0k0\}$ , they display a bi-exponential decay up to  $\sim 20$  ps followed by a long timescale recovery. ZZ reflections  $\{h00\}$  exhibit a similar intensity drop on a fast timescale while showing a pronounced difference in the second slow process with an anomalous fast recovery on a ~20 ps timescale, much faster than expected thermal cooling times. Although the relative intensity drops in for AC reflections have a clear O dependence such that higher-order diffraction peaks show larger decreases following a Debye-Waller (DW) behavior<sup>34, 35</sup> (Fig. S1 and Fig. S4a), such extremely fast intensity recovery time-scales have not been observed in prior UED measurements and cannot be simply understood by a DW effect alone which weakens the Bragg intensities due to the increase of random atomic thermal vibrations after photoexcitation<sup>36, 37</sup>, preserving the symmetry of the crystal. Additional lattice distortions must account for this remarkable increase in intensity for ZZ reflections<sup>37-40</sup>.

To quantitatively model the full dynamic response across all measured timescales, we propose a structural model which incorporates both unit cell symmetry distortions and the effect of thermal vibrations into the structure factor  $F_{hkl}$ . We first consider an anisotropic DW temperature factor (see Supplementary S1.1 and S1.2). For GeS in-plane Bragg reflections (hk0), we observe a DW-like dependence in the first process (t  $\sim 1.5$  ps) in which the relative intensity  $\frac{I_{hk0}(\Delta t)}{I_{hk0}^0} =$ changes an anisotropic DW be understood factor can  $e^{-[\Delta\langle u_{h00}^2\rangle(\Delta t)\cdot Q_{h00}^2+\Delta\langle u_{0k0}^2\rangle(\Delta t)\cdot Q_{0k0}^2]}$ , where  $I_{hkl}^0$  is the unpumped diffraction signal, h,k,l are Miller indices,  $\Delta \langle u_{h00}^2 \rangle$  and  $\Delta \langle u_{0k0}^2 \rangle$  correspond to the change of anisotropic atomic mean squared displacement (MSD) parameters in the ZZ and AC directions. The logarithm of the maximum relative intensity changes of the AC and ZZ peaks in the first process are linearly related to  $Q^2$  as shown in the inset of Fig. 3b. In addition, both AC and ZZ reflections exhibit similar MSD dynamics with a different magnitude for the first fast process (Fig. S2). These observations suggest that the first process is dominated by the DW effect. To further validate this argument, we calculate the MSDs along all in-plane directions according to the anisotropic MSDs of  $\{h00\}$  and  $\{0k0\}$  at  $t \sim 1.5$  ps, finding  $\Delta \langle u_{0k0}^2 \rangle \approx 1.8 \Delta \langle u_{h00}^2 \rangle$ . We introduce an anisotropic factor  $\alpha$  for scaling all other Bragg reflections  $\{hk0\}$  by assuming  $\Delta \langle u_{0k0}^2 \rangle = \alpha^2 \Delta \langle u_{h00}^2 \rangle$ , then the logarithm of the relative intensity changes of  $\{hk0\}$  reflections can be written:

$$ln\left[\frac{I_{hk0}(\Delta t)}{I_{hk0}^{0}}\right] = -\Delta \langle u_{h00}^{2} \rangle (\Delta t) \cdot \left(Q_{h00}^{2} + \left(\alpha Q_{0k0}\right)^{2}\right) = -\Delta \langle u_{h00}^{2} \rangle (\Delta t) \cdot Q_{S}^{2} \tag{1}$$

where  $Q_S^2 = Q_{h00}^2 + (\alpha Q_{0k0})^2$  is the scaled  $Q^2$  (see Supplementary S1.3 for details). As shown in Fig. 3b, this collapses all measured peaks to a single line when plotted versus  $Q_S^2$ .

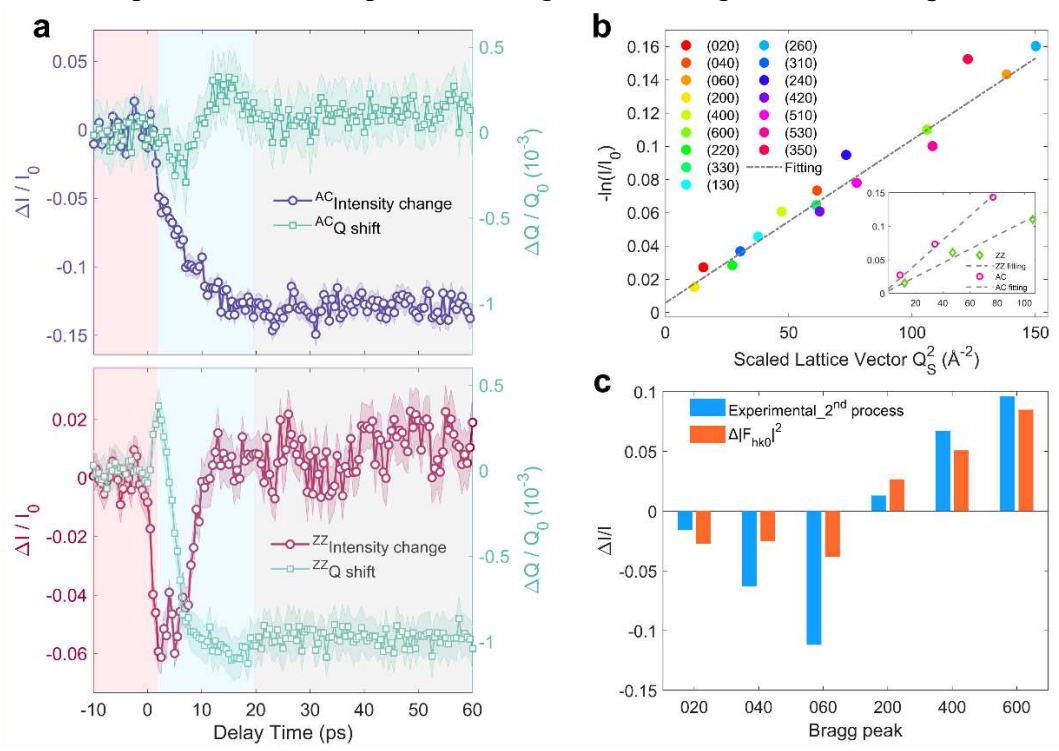


Fig. 3 Analysis of transient changes in Bragg peak intensities. (a) Anisotropic time-dependent diffracted intensity changes for armchair (AC) and zigzag (ZZ) Bragg reflections overlaid with their corresponding Q shift. These changes can be divided into three timescales: 1) the first 1.5 ps in light red background; 2) 1.5 ps to 20 ps in light blue background; 3) after 20 ps in light grey background. (b) The negative logarithm of the maximum relative intensity changes of all in-plane reflections vs. scaled scattering vector squared. It shows a linear dependence on the scaled  $Q^2$ , that is, it mainly follows a Debye-Waller-like dependence in the first  $\sim$ 1.5 ps. Inset shows the same analysis for AC and ZZ peaks vs. unscaled  $Q^2$ . (c) Comparison of the second timescale intensity change between experiment and calculations based on the structure factor model, which shows good agreement.

The second process (1.5 ps < t < 20 ps), as discussed above, is dominated by the additional unit-cell structure change. The relative intensity change of in-plane reflections can be simplified to (see Supplementary S1.4):

$$\frac{I_{hk0}(\Delta t)}{I_{hk0}^{0}} = \frac{\left| \sum_{j=1}^{N} f_{j}(Q_{hk0}(\Delta t)) \cdot e^{-2\pi i \left(x_{j}(\Delta t)h + y_{j}(\Delta t)k\right)} \right|^{2}}{\left| \sum_{j=1}^{N} f_{j}(Q_{hk0}(t_{0})) \cdot e^{-2\pi i \left(x_{j}(t_{0})h + y_{j}(t_{0})k\right)} \right|^{2}}$$
(2)

where N is the number of atoms in the unit cell,  $x_i$ ,  $y_i$  are the positional coordinates of the jth atom,

and the atomic scattering factor  $f_j(Q_{hkl}) = \sum_{n=0}^{5} a_{n,j} \cdot e^{-b_{n,j} \cdot \frac{Q_{hkl}^2}{16\pi^2}}$  is obtained from the scattering parameterization calculated by Peng et al.<sup>41</sup>. According to Eq. 2, only light-induced in-plane atomic displacements  $(\Delta x_j, \Delta y_j)$  and a change in  $Q_{hk0}$  (associated with modulations in  $d_{hk0}$ ) can modulate the time-dependent diffraction intensity<sup>42</sup>.

Since pure ZZ peaks (h00) show unusual fast recovery behavior, we first examine their intensity change by displacing the Ge atoms (and S atoms) along the ZZ direction from their equilibrium positions. Based on the atomic fractional coordinates in the unit cell, the structure factor before and after displacements indicate  $|F_{200,after}| \le |F_{200,before}|$  according to Eq. 13 and Eq.14 in Supplementary S1.4, which means the anomalous fast recovery in ZZ reflections is not caused by only changing the displacements along the ZZ direction (see Supplementary S1.4 and Fig. S3). We further modify the  $Q_{hk0}$  according to the Q shift along the ZZ and AC directions since the presence of light-induced long-range strain shifts the Bragg peak from its strain-free center position  $Q_0$  to a new coordinate<sup>43</sup>  $(Q_0 + \Delta Q)$ , associated with a changing  $d_{hk0}$ . Interestingly, we find that a slight change of  $Q_{hk0}$  in the form factor can lead to a similar 2D difference map as shown in Fig. 2b and Fig.2c (Fig. S3). We find that the amplitude of each peak's intensity modulation is proportional to the Q shift (see Supplementary S1.4 for details). With  $\sim 10$  times bigger Q shift, the calculated  $\frac{\Delta I_{hk0}}{I_{hk0}^0}$  based on the structure factor model is roughly consistent with the amplitude of the experimental intensity change of the second process (Fig. 3c). Although a larger strain is needed to match the calculation and experiment quantitatively, the actual local strain level in the pumped region may be greater than the 0.1% value extracted due to inhomogeneity in the strain response and additional motion in the out-of-plane direction (e.g., dynamic rippling of the flake) not resolved here. This is discussed below regarding the transient peak broadening. These observations suggest that the unusual intensity rise in the ZZ direction is related to the observed ultrafast light-induced strain in the 1.5 ps to 16 ps interval. The strong correlation between the relative intensity change and Q shift can be seen by plotting them together (Fig. 3a), providing further support that the dynamic strain response underlies the resolved changes in diffraction intensity. We conclude that both the thermal vibrations and lattice distortions/strains contribute to the ultrafast intensity variations, and they play a dominant role in the first and second process, respectively.

We further studied the peak width change  $\Delta\omega$  to identify the spatial variation of the strain. Interestingly, no obvious peak width change takes place along the AC direction over the whole delay ranges, while a broadening of the ZZ Bragg peaks (h00) is observed to almost linearly increase up to ~16 ps and last over 100 ps (Fig. S5). Following earlier work<sup>33</sup>, this anisotropic ~1% peak width broadening indicates that the ZZ lattices experience more pronounced inhomogeneous lattice distortions upon photoexcitation and implies dynamic strain-induced rippling (e.g., out of plane motion) which must be occurring for the in-plane strain to respond so quickly. Our experimental observation of no broadening in the AC direction (e.g., no rippling) is also consistent

with the theoretical predictions that there is more flexibility in adjusting the AC direction due to the puckered structure with coupled hinge-like bonding configurations<sup>44-46</sup>.

In order to understand the microscopic origin of the ultrafast photo-induced anisotropic deformation of the lattice, we consider three possible mechanisms<sup>7, 8, 47</sup>: (i) thermal expansion following light-induced lattice heating<sup>16</sup>, associated with a thermal stress  $\Delta s_{th}$ , (ii) deformation potential coupling (also termed electronic pressure)<sup>20, 21, 48, 49</sup> created by the electronic density redistribution upon excitation,  $\Delta s_{DP}$ , and (iii) the converse piezoelectric effect (CPE) generated by a photoinduced electric field<sup>29, 50, 51</sup>,  $\Delta s_{CPE}$ .

First, the most obvious factor is the thermal contribution resulting from temperature changes induced by above-gap absorption. X-ray studies of the lattice parameters of GeS as a function of temperature<sup>52</sup> suggest both ZZ and AC expand when heating to ~518 K which is inconsistent with our observations that the ZZ lattice vector contracts within the first 1.5 ps (Fig. 2d). We further performed in-situ heating measurements in a transmission electron microscopy (TEM) setup to understand the contribution from the thermal expansion. No similar difference map (473 K – 300 K) as Fig. 2a can be obtained (Fig. S6), again suggesting the response is not dominated by thermal effects. We conclude that strain due to laser-induced thermal expansion cannot be the main cause of photostriction.

We further consider the possible contribution from a nonthermal deformation potential mechanism, which relates-uniaxial strains ( $\varepsilon_{zz}$  and  $\varepsilon_{AC}$ ) to band-edge shifts, by density functional theory calculations. For above-bandgap excitation in a semiconductor (Fig.4a), the photogeneration of free charge carriers modulates the electron-density the band structure, resulting in the development of a local photoinduced mechanical stress  $\Delta s_{DP}$  which is proportional to  $\frac{\partial E_g}{\partial P_r} \Delta n^{21, 48, 53}$ , where  $\frac{\partial E_g}{\partial P_r}$  is the pressure dependence of the bandgap energy and  $\Delta n$  is the photogenerated excess charge carriers. When  $\frac{\partial E_g}{\partial P_r}$  is negative, the photoinduced stress will tend to make the crystal contract; when  $\frac{\partial E_g}{\partial P_r}$  is positive, the photoinduced stress will tend to make the crystal expand<sup>48</sup>.  $\varepsilon_{zz}$  and  $\varepsilon_{AC}$  result in different bandgap deformation potentials, showing a positive  $\frac{\partial E_g}{\partial \varepsilon_{zz}}$  and a negative  $\frac{\partial E_g}{\partial \varepsilon_{AC}}$  (Fig. 4b). Since positive  $\varepsilon$  corresponds to tensile strain, the sign of  $\frac{\partial E_g}{\partial \varepsilon}$  is opposite to  $\frac{\partial E_g}{\partial P_r}$ . The negative  $\frac{\partial E_g}{\partial P_r}$  for ZZ direction (positive  $\frac{\partial E_g}{\partial P_r}$  for AC directions) agrees well with the initial lattice contraction (expansion) observed along the ZZ (AC) direction.

Although the deformation potential mechanism is consistent with the first fast process, it cannot explain the second process (t>1.5 ps), in which the ZZ axis expands and AC axis contracts. As pointed out previously, such unusual anisotropic lattice changes have been predicted in monolayer ferroelectric  $MX^{29}$ , which is attributed to the screening of polarization caused by photoinduced electric field and mediated by the CPE. After checking the calculation method by repeating predicted results for monolayer GeS, we further investigated the behavior of bulk multilayer GeS. Based on the analysis of the potential direct optical transitions along the band structure, we calculated the photoinduced nonthermal change of a (ZZ) and b (AC) axes at three

different k-points as a function of free carrier densities for bulk GeS, namely  $\Gamma$ , YI, and Y2, where the optical transitions are most likely to happen. Such optical processes can only be allowed for interband transitions with nonzero dipole matrix elements. From the orbital characters of the band structure shown in Fig. 4c, the nonzero matrix element can originate from the s orbital in the valence band edges, and the  $p_y$  orbitals in the conduction band edges, along  $\Gamma - Y$  path. It agrees well with the wavefunctions of the conduction band minimum (CBM) and valence band maximum (VBM) in Fig. 4d for YI and Y2 k-points, where the wavefunction of the CBM show in-plane Ge- $p_y$  orbital characters, while that of the VBM is dominated by the Ge-s and S-s s0 orbitals.

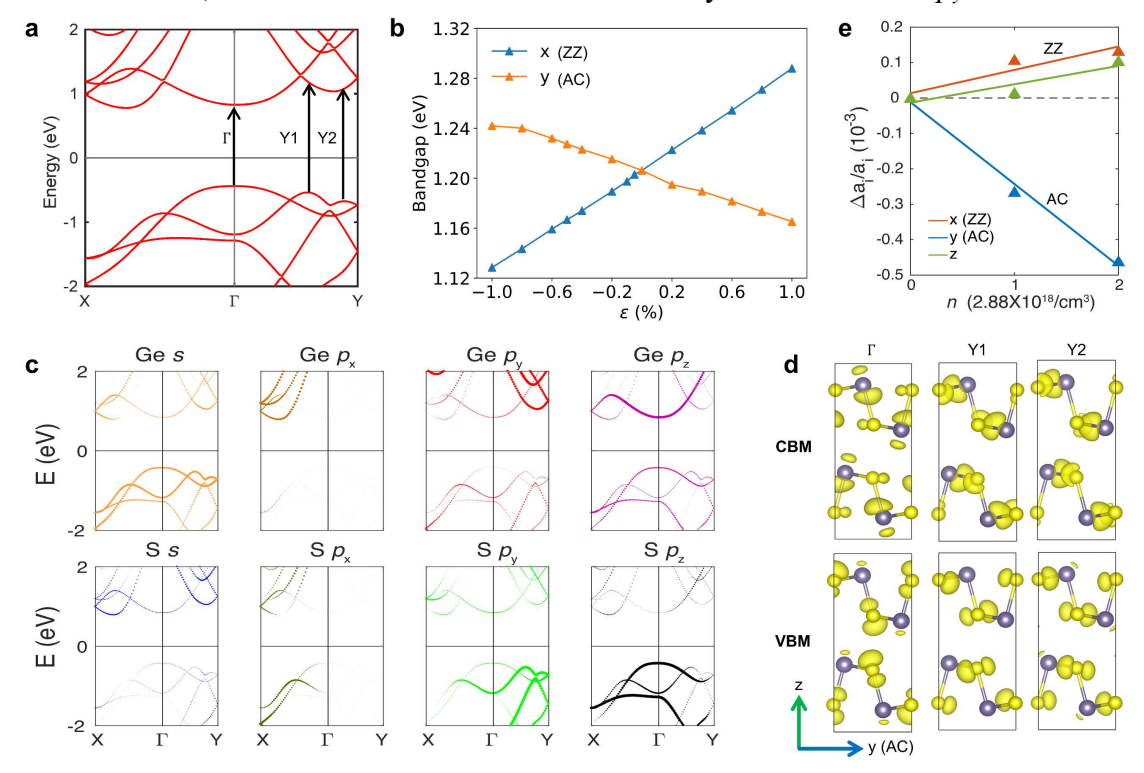


Fig. 4 Microscopic pictures of photo-induced anisotropic dynamics in GeS. (a) The band structure of bulk GeS. (b) The changes of band gap under uniaxial strain, illustrating the deformation potential along the ZZ and AC directions. (c) Orbital characters along the band structure high symmetry path of the band structure. (d) Partial charge density of the valence and conduction band edges for three special k points at  $\Gamma$ , YI, and Y2. (e) The average change of lattice parameters as a function of carrier density.

The variations of the structure with carrier density is shown in Fig. S8, and the average of the lattice deformations induced by the three transitions is shown in Fig. 4e. The in-plane lattice parameters a and b exhibit anisotropic variations such that the lattice constant of the long axis b shows a linear contraction while the short-axis a exhibits a linear expansion as the photoexcited carrier density increases (Fig. 4e), consistent with the experimental measurements. Although in the bulk (for even number of layers) there is no net ferroelectricity due to the canceling polarization between adjacent layers, the lattice constant is also stretched along the polarization vector within

each layer and still prone to photostriction. As discussed previously, the thermal-induced strain is a small contribution compared to other effects. As for the deformation potential, it competes with the lattice change caused by CPE and favors shrinking along the ZZ direction. As a result, for the first process within  $\sim 1.5$  ps, the deformation potential is the dominant mechanism while the CPE dominates for longer timescales.

In summary, we observed a pronounced dynamic anisotropic strain between the AC and ZZ directions induced by electronic excitation. GeS dynamically shrinks along its polarization axis, while the direction perpendicular to the polarization stretches under carrier excitation. The origin of the large photostriction in GeS is found to arise not only from converse piezoelectric effects; rather the contribution of the deformation potential must be accounted for at short time scales. Further study of the polarization dependence of the photostrictive response is important to enable independent control of the strain response along the AC vs. ZZ directions. These results experimentally demonstrate the photostrictive effect in 2D layered MXs. Although prior theoretical studies have focused on monolayer photostrictive responses, our results show these effects are also present in the multilayer, antiferroelectrically coupled limit, which is important for simplifying material requirements towards applications based on this effect. The realization of photo-induced strain in layered GeS opens an unexplored possibility for ultrafast strain engineering in functional devices and exploration of photostrictive effects in layered antiferroelectrics and other 2D materials in the future.

## ASSOCIATED CONTENT

**Supporting Information.** The Supporting Information is available free of charge. It includes experimental materials and methods; structure factor and temperature effect model for anisotropic GeS; and supplementary Fig. 1 to 8 (PDF)

## **AUTHOR INFORMATION**

## **Corresponding Author**

Aaron Lindenberg - Department of Materials Science and Engineering, Stanford University, Stanford, California 94305, USA. Email: aaronl@stanford.edu

## **Author contributions**

D.L., E.J.S. and A.M.L. designed the research. E.J.S., C.M.N., X.Z.S., X.J.W., A.H.R. and S.W. performed the UED experiments with the laser help of M.C.H.. D.L. processed the UED data. D.L. and A.M.L. analyzed the data and discussed the results. B.Y.Z. and X.F.Q. performed the DFT calculations. Q.Y.F. helped on the optical experiments. J.G.W. helped on the in-situ TEM heating

experiments. D.L. and A.M.L. wrote the manuscript with discussion and improvements from all authors.

## **ACKNOWLEDGMENTS**

We thank Dr. Jie Yang and Dr. Michael E. Kozina for their help on the experiments. This work is supported by the Department of Energy, Office of Science, Basic Energy Sciences, Materials Sciences and Engineering Division, under Contract DE-AC02-76SF00515. The MeV-UED experiments were carried out at SLAC MeV-UED. SLAC MeV-UED is supported in part by the DOE BES SUF Division Accelerator & Detector R&D program, the LCLS Facility, and SLAC under Contract Nos. DE-AC02-05-CH11231 and DE-AC02-76SF00515. X.F.Q. acknowledges the support by the US National Science Foundation (NSF) under award number DMR-2103842. B.Y.Z. acknowledges the support by the US NSF under award number DMR-1753054. Portions of this research were conducted with the advanced computing resources provided by Texas A&M High Performance Research Computing.

## **REFERENCES**

- (1) Zhou, J.; Xu, H.; Li, Y.; Jaramillo, R.; Li, J., Opto-mechanics driven fast martensitic transition in two-dimensional materials. *Nano Lett* **2018**, *18* (12), 7794-7800.
- (2) Xu, H.; Zhou, J.; Li, Y.; Jaramillo, R.; Li, J., Optomechanical control of stacking patterns of h-BN bilayer. *Nano Research* **2019**, *12* (10), 2634-2639.
- (3) Zhou, J.; Zhang, S.; Li, J., Normal-to-topological insulator martensitic phase transition in group-IV monochalcogenides driven by light. *NPG Asia Materials* **2020**, *12* (1), 1-9.
- (4) Zhou, J.; Mao, S.; Zhang, S., Noncontacting optostriction driven anisotropic and inhomogeneous strain in two-dimensional materials. *Physical Review Research* **2020**, *2* (2), 022059.
- (5) Disa, A. S.; Nova, T. F.; Cavalleri, A., Engineering crystal structures with light. *Nature Physics* **2021**, *17* (10), 1087-1092.
- (6) Bao, C.; Tang, P.; Sun, D.; Zhou, S., Light-induced emergent phenomena in 2D materials and topological materials. *Nature Reviews Physics* **2021**, 1-16.
- (7) Chen, C.; Yi, Z., Photostrictive Effect: Characterization Techniques, Materials, and Applications. *Advanced Functional Materials* **2021**, *31* (22), 2010706.
- (8) Kundys, B., Photostrictive materials. *Applied Physics Reviews* **2015**, *2* (1), 011301.
- (9) Poosanaas, P.; Tonooka, K.; Uchino, K., Photostrictive actuators. *Mechatronics* **2000**, *10* (4-5), 467-487.
- (10) Lafont, T.; Gimeno, L.; Delamare, J.; Lebedev, G.; Zakharov, D.; Viala, B.; Cugat, O.; Galopin, N.; Garbuio, L.; Geoffroy, O., Magnetostrictive–piezoelectric composite structures for energy harvesting. *J Micromech Microeng* **2012**, *22* (9), 094009.

- (11) Tsai, H.; Asadpour, R.; Blancon, J.-C.; Stoumpos, C. C.; Durand, O.; Strzalka, J. W.; Chen, B.; Verduzco, R.; Ajayan, P. M.; Tretiak, S., Light-induced lattice expansion leads to high-efficiency perovskite solar cells. *Science* **2018**, *360* (6384), 67-70.
- (12) Li, W.; Sidhik, S.; Traore, B.; Asadpour, R.; Hou, J.; Zhang, H.; Fehr, A.; Essman, J.; Wang, Y.; Hoffman, J. M., Light-activated interlayer contraction in two-dimensional perovskites for high-efficiency solar cells. *Nat Nanotechnol* **2021**, 1-8.
- (13) Tatsuzaki, I.; Itoh, K.; Ueda, S.; Shindo, Y., Strain along c axis of SbSI caused by illumination in dc electric field. *Physical Review Letters* **1966**, *17* (4), 198.
- (14) Kundys, B.; Viret, M.; Colson, D.; Kundys, D. O., Light-induced size changes in BiFeO 3 crystals. *Nat Mater* **2010**, *9* (10), 803-805.
- (15) Daranciang, D.; Highland, M. J.; Wen, H.; Young, S. M.; Brandt, N. C.; Hwang, H. Y.; Vattilana, M.; Nicoul, M.; Quirin, F.; Goodfellow, J., Ultrafast photovoltaic response in ferroelectric nanolayers. *Physical review letters* **2012**, *108* (8), 087601.
- (16) Wen, H.; Chen, P.; Cosgriff, M. P.; Walko, D. A.; Lee, J. H.; Adamo, C.; Schaller, R. D.; Ihlefeld, J. F.; Dufresne, E. M.; Schlom, D. G., Electronic origin of ultrafast photoinduced strain in BiFeO 3. *Physical review letters* 2013, 110 (3), 037601.
- (17) Schick, D.; Herzog, M.; Wen, H.; Chen, P.; Adamo, C.; Gaal, P.; Schlom, D. G.; Evans, P. G.; Li, Y.; Bargheer, M., Localized excited charge carriers generate ultrafast inhomogeneous strain in the multiferroic BiFeO 3. *Physical review letters* **2014**, *112* (9), 097602.
- (18) Matzen, S.; Guillemot, L.; Maroutian, T.; Patel, S. K.; Wen, H.; DiChiara, A. D.; Agnus, G.; Shpyrko, O. G.; Fullerton, E. E.; Ravelosona, D., Tuning Ultrafast Photoinduced Strain in Ferroelectric-Based Devices. *Advanced Electronic Materials* **2019**, *5* (6), 1800709.
- (19) Lagowski, J.; Gatos, H., Photomechanical Effect in Noncentrosymmetric Semiconductors-CdS. *Applied Physics Letters* **1972**, *20* (1), 14-16.
- (20) Figielski, T., Photostriction effect in germanium. *physica status solidi (b)* **1961,** *l* (4), 306-316.
- (21) Gauster, W.; Habing, D., Electronic volume effect in silicon. *Physical Review Letters* **1967**, *18* (24), 1058.
- (22) Yu, Y.; Nakano, M.; Ikeda, T., Directed bending of a polymer film by light. *Nature* **2003**, *425* (6954), 145-145.
- (23) Finkelmann, H.; Nishikawa, E.; Pereira, G.; Warner, M., A new opto-mechanical effect in solids. *Physical Review Letters* **2001**, *87* (1), 015501.
- (24) Zhou, Y.; You, L.; Wang, S.; Ku, Z.; Fan, H.; Schmidt, D.; Rusydi, A.; Chang, L.; Wang, L.; Ren, P., Giant photostriction in organic–inorganic lead halide perovskites. *Nat Commun* **2016**, *7* (1), 1-8.
- (25) Wei, T. C.; Wang, H. P.; Li, T. Y.; Lin, C. H.; Hsieh, Y. H.; Chu, Y. H.; He, J. H., Photostriction of CH3NH3PbBr3 perovskite crystals. *Adv Mater* **2017**, *29* (35), 1701789.
- (26) Wang, Y.; Liu, C.; Ren, Y.; Zuo, X.; Canton, S. E.; Zheng, K.; Lu, K.; Lü, X.; Yang, W.; Zhang, X., Visualizing Light-Induced Microstrain and Phase Transition in Lead-Free

- Perovskites Using Time-Resolved X-Ray Diffraction. *Journal of the American Chemical Society* **2022**.
- (27) Wei, T.-C.; Wang, H.-P.; Liu, H.-J.; Tsai, D.-S.; Ke, J.-J.; Wu, C.-L.; Yin, Y.-P.; Zhan, Q.; Lin, G.-R.; Chu, Y.-H., Photostriction of strontium ruthenate. *Nat Commun* 2017, 8 (1), 1-8.
- (28) Li, X.; Chen, C.; Zhang, F.; Fang, H.; Huang, X.; Yi, Z., Photostriction of Ferrites Under Visible Light. *ACS Applied Electronic Materials* **2021**.
- (29) Haleoot, R.; Paillard, C.; Kaloni, T. P.; Mehboudi, M.; Xu, B.; Bellaiche, L.; Barraza-Lopez, S., Photostrictive two-dimensional materials in the monochalcogenide family. *Physical review letters* **2017**, *118* (22), 227401.
- (30) Barraza-Lopez, S.; Fregoso, B. M.; Villanova, J. W.; Parkin, S. S.; Chang, K., Colloquium: Physical properties of group-IV monochalcogenide monolayers. *Reviews of Modern Physics* **2021**, *93* (1), 011001.
- (31) Kundys, B.; Viret, M.; Meny, C.; Da Costa, V.; Colson, D.; Doudin, B., Wavelength dependence of photoinduced deformation in BiFeO 3. *Physical Review B* **2012**, *85* (9), 092301.
- (32) Yan, Y.; Deng, Q.; Li, S.; Guo, T.; Li, X.; Jiang, Y.; Song, X.; Huang, W.; Yang, J.; Xia, C., In-plane ferroelectricity in few-layered GeS and its van der Waals ferroelectric diodes. *Nanoscale* **2021**, *13* (38), 16122-16130.
- (33) Mannebach, E. M.; Li, R.; Duerloo, K.-A.; Nyby, C.; Zalden, P.; Vecchione, T.; Ernst, F.; Reid, A. H.; Chase, T.; Shen, X., Dynamic structural response and deformations of monolayer MoS2 visualized by femtosecond electron diffraction. *Nano Lett* 2015, 15 (10), 6889-6895.
- (34) Zahn, D.; Hildebrandt, P.-N.; Vasileiadis, T.; Windsor, Y. W.; Qi, Y.; Seiler, H. l. n.; Ernstorfer, R., Anisotropic Nonequilibrium Lattice Dynamics of Black Phosphorus. *Nano Lett* **2020**, *20* (5), 3728-3733.
- (35) Peng, L.-M., Electron atomic scattering factors and scattering potentials of crystals. *Micron* **1999**, *30* (6), 625-648.
- (36) René de Cotret, L. P.; Otto, M. R.; Pöhls, J.-H.; Luo, Z.; Kanatzidis, M. G.; Siwick, B. J., Direct visualization of polaron formation in the thermoelectric SnSe. *Proceedings of the National Academy of Sciences* **2022**, *119* (3), e2113967119.
- (37) Wang, W.; Wu, L.; Li, J.; Aryal, N.; Jin, X.; Liu, Y.; Fedurin, M.; Babzien, M.; Kupfer, R.; Palmer, M., Photoinduced anisotropic lattice dynamic response and domain formation in thermoelectric SnSe. *npj Quantum Materials* **2021**, *6* (1), 1-8.
- (38) Reid, A.; Shen, X.; Maldonado, P.; Chase, T.; Jal, E.; Granitzka, P.; Carva, K.; Li, R.; Li, J.; Wu, L., Beyond a phenomenological description of magnetostriction. *Nat Commun* **2018**, *9* (1), 1-9.
- (39) Jiang, Y.; Liu, L. C.; Sarracini, A.; Krawczyk, K. M.; Wentzell, J. S.; Lu, C.; Field, R. L.; Matar, S. F.; Gawelda, W.; Müller-Werkmeister, H. M., Direct observation of nuclear reorganization driven by ultrafast spin transitions. *Nat Commun* 2020, 11 (1), 1-8.

- (40) Konstantinova, T.; Wu, L.; Yin, W.-G.; Tao, J.; Gu, G.; Wang, X.; Yang, J.; Zaliznyak, I.; Zhu, Y., Photoinduced Dirac semimetal in ZrTe 5. *npj Quantum Materials* **2020**, *5* (1), 1-8.
- (41) Peng, L.-M.; Ren, G.; Dudarev, S.; Whelan, M., Robust parameterization of elastic and absorptive electron atomic scattering factors. *Acta Crystallographica Section A: Foundations of Crystallography* **1996**, *52* (2), 257-276.
- (42) Peter Blaha, R. N., Valerio Olevano, Bruce D. Patterson, Sebastien Pillet and Karlheinz Schwarz, *Structures on Different Time Scales*, *Volume 1*. De Gruyter: 2018.
- (43) Boulle, A.; Chartier, A.; Debelle, A.; Jin, X.; Crocombette, J.-P., Computational diffraction reveals long-range strains, distortions and disorder in molecular dynamics simulations of irradiated single crystals. *Journal of Applied Crystallography* **2022**, *55* (2), 296-309.
- (44) Kou, L.; Ma, Y.; Smith, S. C.; Chen, C., Anisotropic ripple deformation in phosphorene. *The journal of physical chemistry letters* **2015**, *6* (9), 1509-1513.
- (45) Yang, Y.; Zong, H.; Sun, J.; Ding, X., Rippling ferroic phase transition and domain switching in 2D materials. *Adv Mater* **2021**, *33* (49), 2103469.
- (46) Roll, J. E.; Davis, J. M.; Villanova, J. W.; Barraza-Lopez, S., Elasticity of two-dimensional ferroelectrics across their paraelectric phase transformation. *Physical Review B* **2022**, *105* (21), 214105.
- (47) Yang, Y.; Paillard, C.; Xu, B.; Bellaiche, L., Photostriction and elasto-optic response in multiferroics and ferroelectrics from first principles. *Journal of Physics: Condensed Matter* **2018**, *30* (7), 073001.
- (48) Datskos, P. G.; Rajic, S.; Datskou, I., Photoinduced and thermal stress in silicon microcantilevers. *Applied Physics Letters* **1998**, 73 (16), 2319-2321.
- (49) Hu, H.; Liu, M.; Wang, Z.; Zhu, J.; Wu, D.; Ding, H.; Liu, Z.; Liu, F., Quantum electronic stress: Density-functional-theory formulation and physical manifestation. *Physical review letters* **2012**, *109* (5), 055501.
- (50) Paillard, C.; Xu, B.; Dkhil, B.; Geneste, G.; Bellaiche, L., Photostriction in ferroelectrics from density functional theory. *Physical review letters* **2016**, *116* (24), 247401.
- (51) Paillard, C.; Prosandeev, S.; Bellaiche, L., Ab initio approach to photostriction in classical ferroelectric materials. *Physical Review B* **2017**, *96* (4), 045205.
- (52) Wiedemeier, H.; Siemers, P., The thermal expansion of GeS and GeTe. *Z Anorg Allg Chem* **1977**, *431* (1), 299-304.
- (53) Stearns, R.; Kino, G., Effect of electronic strain on photoacoustic generation in silicon. *Applied Physics Letters* **1985**, *47* (10), 1048-1050.

## **TOC Graphic**

